PNAS RESEARCH ARTICLE | CELL BIOLOGY OPEN ACCESS

Autonomous multicolor bioluminescence imaging in bacteria, mammalian, and plant hosts

Subhan Hadi Kusuma[a,b], Taishi Kakizuka[b,c], Mitsuru Hattori[b], and Takeharu Nagai[a,b,c,d,1]

Edited by Nathan Shaner, University of California San Diego, La Jolla, CA; received March 28, 2024; accepted August 27, 2024 by Editorial Board Member James J. Collins

Bioluminescence imaging has become a valuable tool in biological research, offering several advantages over fluorescence-based techniques, including the absence of phototoxicity and photobleaching, along with a higher signal-to-noise ratio. Common bioluminescence imaging methods often require the addition of an external chemical substrate (luciferin), which can result in a decrease in luminescence intensity over time and limit prolonged observations. Since the bacterial bioluminescence system is genetically encoded for luciferase-luciferin production, it enables autonomous bioluminescence (auto-bioluminescence) imaging. However, its application to multiple reporters is restricted due to a limited range of color variants. Here, we report five-color auto-bioluminescence system named Nano-lanternX (NLX), which can be expressed in bacterial, mammalian, and plant hosts, thereby enabling auto-bioluminescence in various living organisms. Utilizing spectral unmixing, we achieved the successful observation of multicolor auto-bioluminescence, enabling detailed single-cell imaging across both bacterial and mammalian cells. We have also expanded the applications of the NLX system, such as multiplexed auto-bioluminescence imaging for gene expression, protein localization, and dynamics of biomolecules within living mammalian cells.

bioluminescence | bacterial luciferase | biosensor | bioimaging

Significance

Autonomous bioluminescence imaging has become an ideal technique for convenient and prolonged observation of cellular events without the addition of a substrate. However, the application of this technology is limited to blue light for bacterial luciferase and green light for fungal luciferase. Here, we report the development of five color variants of autonomous bioluminescence systems using bacterial luciferase. These color variants are expressed not only in bacteria but also in mammalian and plant hosts. Additionally, we extended the application including the visualization of dynamics of gene expression, and bioactive ion and molecule such as $Ca^{2+}$and adenosine triphosphate (ATP).

Bioluminescence is the production of light through an enzymatic reaction involving the oxidation of a chemical substrate (luciferin) by an enzyme (luciferase) (1). The light produced by bioluminescent reactions is widely used to observe biological phenomena in living cells. To enable real-time imaging, continuous addition of luciferin is required. In some luciferin, such as *Renilla* luciferase's luciferin (coelenterazine/CTZ), continuous addition of CTZ leads to increased CTZ's autooxidation (2), lowering the signal-to-noise ratio and complicating long-term imaging. To overcome this issue, efforts have been made to produce luciferin-related genes to create autonomous bioluminescence (auto-bioluminescence) systems. Bacterial luciferases (Lux) and fungal luciferases (Luz) are the only well-known auto-bioluminescence systems, but Luz activity significantly decreases at high temperatures, specifically at 37 °C (3), limiting its usability in mammalian cell imaging. In contrast, Lux, particularly the variant from *Photorhabdus luminescens*, demonstrates thermostability at 37 °C (4), making it more suitable for such applications.

Lux is a heterodimeric luciferase composed of LuxA and LuxB subunits. It generates blue-green light (490 nm) by oxidizing reduced flavin mononucleotide ($FMNH_2$, produced by flavin reductase/Frp) and long-chain fatty aldehyde (RCHO, produced by LuxCDE enzymes) to flavin mononucleotide (FMN) and to carboxylic acid (RCOOH), respectively (4). However, when observing multiple biological events, Lux-based probes cannot be used due to the lack of distinct color variants compared to commonly modified luciferases (5, 6). Consequently, there is considerable demand for Lux color variants to enable monitoring of diverse biological events. Previous color variants of Lux, with a small emission shifted (4 to 16 nm), typically arise from mutations occurring in the active site of luciferase (7) or through protein-binding interactions with yellow fluorescent protein (YFP) (8, 9) and lumazine protein (LumP) (10, 11). However, these modifications can impact Lux activity, resulting in reduced luminescence (7) and altered thermostability (9–11).

To overcome these limitations, we adopted a bioluminescence resonance energy transfer (BRET) strategy inspired by Nano-lantern development (5, 6, 12). This approach successfully produced multicolor variants of luciferase without compromising its luminescence and thermostability. Here, we introduce the multicolor auto-bioluminescent Lux for multiplexed auto-bioluminescence imaging. The multicolor Lux can be expressed in bacteria, and by utilizing codon-optimized Lux (co Lux) (13), it generates bright multicolor auto-bioluminescence in mammalian and plant hosts. These color variants enable the

Author affiliations: [a]Graduate School of Frontier Biosciences, Osaka University, Suita, Osaka 565-0871, Japan; [b]Department of Biomolecular Science and Engineering, SANKEN, Osaka University, Ibaraki, Osaka 567-0047, Japan; [c]Transdimensional Life Imaging Division, Institute for Open and Transdisciplinary Research Initiatives, Osaka University, Suita, Osaka 565-0871, Japan; and [d]Research Institute for Electronic Science, Hokkaido University, Sapporo, Hokkaido 001-0020, Japan

Author contributions: S.H.K. and T.N. designed research; S.H.K. performed research; T.K. performed the cardiomyocyte cell culture; S.H.K., M.H., and T.N. analyzed data; and S.H.K. and T.N. wrote the paper.

Competing interest statement: The authors declare that they have patent application fillings to disclose (JP2023-179446).

This article is a PNAS Direct Submission. N.S. is a guest editor invited by the Editorial Board.

[1]To whom correspondence may be addressed. Email: ng1@sanken.osaka-u.ac.jp.

This article contains supporting information online at https://www.pnas.org/lookup/suppl/doi:10.1073/pnas.2406358121/-/DCSupplemental.

Published October 2, 2024.

visualization of multiplex gene reporters and subcellular tags. Additionally, we have developed peptide-based indicators based on the multicolor Lux system.

Results

Development of Multicolor Lux. To change Lux's bioluminescence color, we adopted a BRET strategy using the YFP Venus (14) as the initial BRET acceptor protein (Fig. 1*A*). The effects of BRET with Venus, including modifications, were previously verified (15). Venus was fused to either the N- or C-terminus of the active subunit of Lux (LuxA) to achieve higher BRET efficiency (*SI Appendix*, Fig. S1*A*). To compare the bioluminescence intensities of these fusion proteins without the influence of endogenous FMN/$FMNH_2$ levels, we measured them in purified proteins rather than in cell systems (as previously reported) (15). For bioluminescence measurements, purified Lux and Venus fusions were added to FMN, decanal, and BNAH (16). Unfortunately, the intensities of these fusions were lower than those of wild-type (WT) Lux (*SI Appendix*, Fig. S1*B*). We speculated that unstructured residues from the C-terminus of Venus might affect the activity or protein folding of LuxA. Consequently, deleting Venus's C-terminus (VenusΔC10-LuxA) significantly improved the bioluminescence intensity compared to the WT (*SI Appendix*, Fig. S1*B*). Referring to this structure, except mKOκ (17) (orange FP), which lacks unstructured residues at the C-terminus, the other truncated FPs, including mTurquoise2 (18) (cyan FP), sfGFP (19) (green FP), and mScarlet-I (20) (red FP), were fused with LuxA to serve as BRET acceptors. In the development of the red variant, we initially considered several red fluorescent proteins (FPs) due to the lower spectral overlap between Lux and common red FPs. Among the options, mScarlet-I (20) was chosen because of its higher BRET efficiency compared to CyOFP1 (21), mCherry-XL (22), and Scarlet (20) (*SI Appendix*, Fig. S2 and Table S1).

We also attempted to fuse FPs to the N- or C-terminus of LuxB to assess their suitability for LuxB fusion (15), with the goal of producing a multicolor Lux. However, even in this scenario, the BRET efficiency in the LuxA fusion remained higher than that in the LuxB fusion (*SI Appendix*, Fig. S3 and Table S1). We designated these LuxA-based variants as NLX (Nano-lantern based on Lux luciferase), comprising cyan NLX (CNLX) ($\lambda_{max}^{EM} = 480$ nm), green NLX (GNLX) ($\lambda_{max}^{EM} = 520$ nm), yellow NLX (YNLX) ($\lambda_{max}^{EM} = 534$ nm), orange NLX (ONLX) ($\lambda_{max}^{EM} = 569$ nm), and red NLX (RNLX) ($\lambda_{max}^{EM} = 597$ nm) (Fig. 1 *B* and *C*). The bioluminescence intensities of the purified NLXs exceeded those of the original Lux, although the specific increases varied (Fig. 1*D*). The fusion with FPs increased the luminescent quantum yield (QY), while the enzymatic parameters (k_{cat}) of all NLXs remained similar to those of WT Lux (*SI Appendix*, Fig. S4 *A* and *B* and Table S2). Notably, CNLX exhibited a sixfold higher QY than Lux (*SI Appendix*, Table S2).

In comparison with other non-autobioluminescent proteins, we compared the bioluminescent kinetics and intensity of purified YNL (yellow Nano-lantern, based on RLuc8-S257G), YeNL (yellow enhanced Nano-lantern, based on NanoLuc), Fluc (firefly luciferase), and YNLX proteins. The results showed that YNLX had a longer half-life ($t_{1/2}$) compared to the other proteins tested

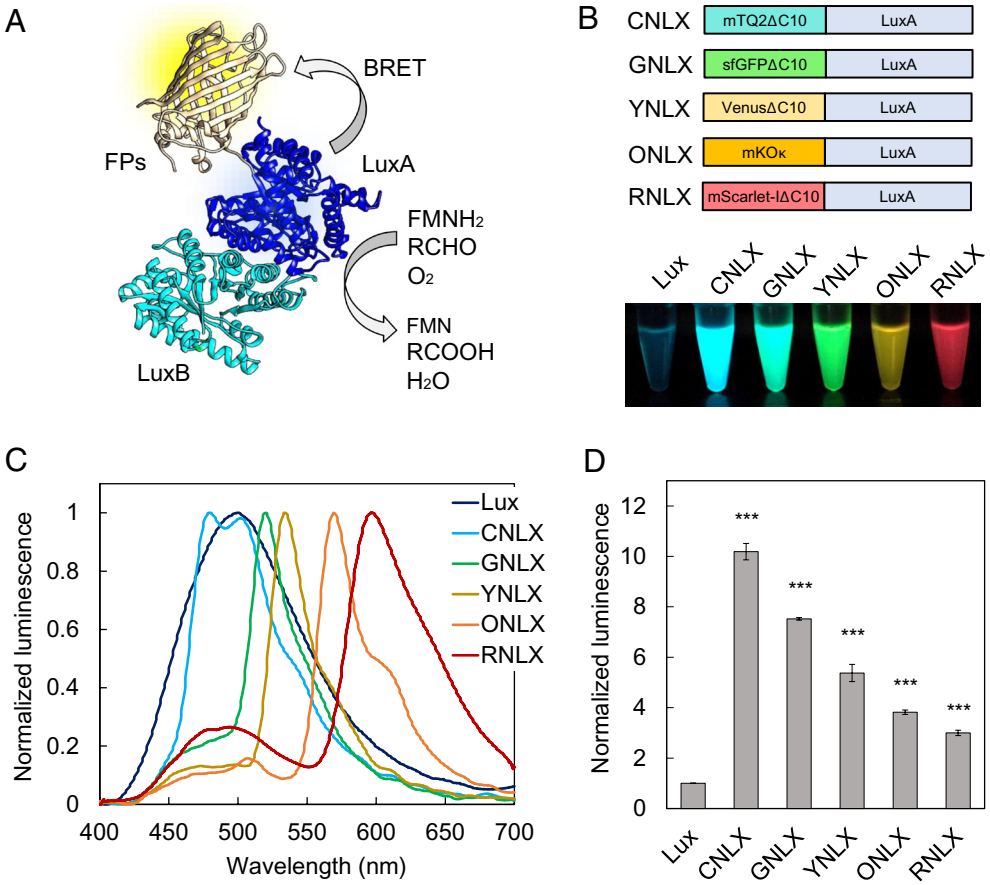

Fig. 1. Development and characterization of NLX. (*A*) Structural model of NLX, consisting of heterodimeric Lux, LuxA (blue), LuxB (cyan), and FP (yellow). (*B*) Schematic of the NLX series (*Upper* panel) and bioluminescence images of recombinant NLXs proteins (*Bottom*). (*C*) Bioluminescence spectra of NLXs proteins. The bioluminescence intensities were normalized to each peak intensity. (*D*) Bioluminescence intensities of NLXs. Comparison of bioluminescence intensities of NLXs proteins and Lux. Data are mean ± SD. $n = 3$, ***$P < 0.001$.

(*SI Appendix*, Fig. S5*A*). In contrast, YeNL exhibited a shorter half-life than the other proteins tested. Additionally, the luminescence intensity of YNLX was comparable to Fluc, although it was lower than that of YNL and YeNL (*SI Appendix*, Fig. S5*B*).

Autonomous Bioluminescence Imaging of NLXs. We next evaluated coexpression of NLXs with luciferin biosynthesis genes, such as *frp* and *luxCDE*, to promote multicolor auto-bioluminescence in various living organisms. Initially, we examined multicolor auto-bioluminescence in bacterial cell hosts by transforming *Escherichia coli* with NLXs and the *luxCDE* operon, both driven by the T7 promoter. The bioluminescence emitted by recombinant *E. coli* expressing individual NLXs exhibited the expected colors, consistent with the bioluminescence observed in NLX-purified proteins (Fig. 2*A*). Additionally, we conducted multiplexed auto-bioluminescence imaging by mixing *E. coli* containing CNLX, YNLX, and RNLX plasmids (Fig. 2*B*). Recombinant *E. coli* demonstrated the capacity to be differentiated by color using specific optical filters and minimizing spectral noise with spectral unmixing algorithms (23). This study marks the first report of multicolor auto-bioluminescent bacteria that have a large spectral range from blue to red.

To evaluate NLXs' performance in mammalian cells, they were introduced into the human co Lux operon (co *luxA*, co *luxB*, co *luxC*, co *luxD*, co *luxE*, and co *Frp*) (13), replacing *luxA* in NLXs with co *luxA*. Since the original co lux expression necessitated cotransfecting six plasmids for each gene, we sought to minimize the number of plasmids by utilizing the 2A peptide to link proteins (*SI Appendix*, Fig. S6*A*). co *luxD*, co *luxE*, and co *luxC* were constructed as a tricistronic unit using two 2A peptides (co *luxD-P2A*-co *luxE-T2A*-co *luxC*) (DEC(2A)). In addition, co *luxB* was fused with co *Frp* using GGGGS (G4S) (24). As a result, the fusion of co *luxB* and co *Frp*, BF(G4S) increased the luminescence intensity in cells compared to that of co lux (*SI Appendix*, Fig. S5*B*). In contrast, DEC(2A) did not enhance the intensity, which was also similarly reported previously (13), Therefore, by introducing the Kozak sequence (25) downstream of the 2A peptide, DEC(KZK) (*SI Appendix*, Fig. S6*A*), the luminescence intensity was improved (*SI Appendix*, Fig. S5*B*). The optimized co lux operon-expressing plasmids, BF(G4S) and DEC(KZK), were cotransfected with

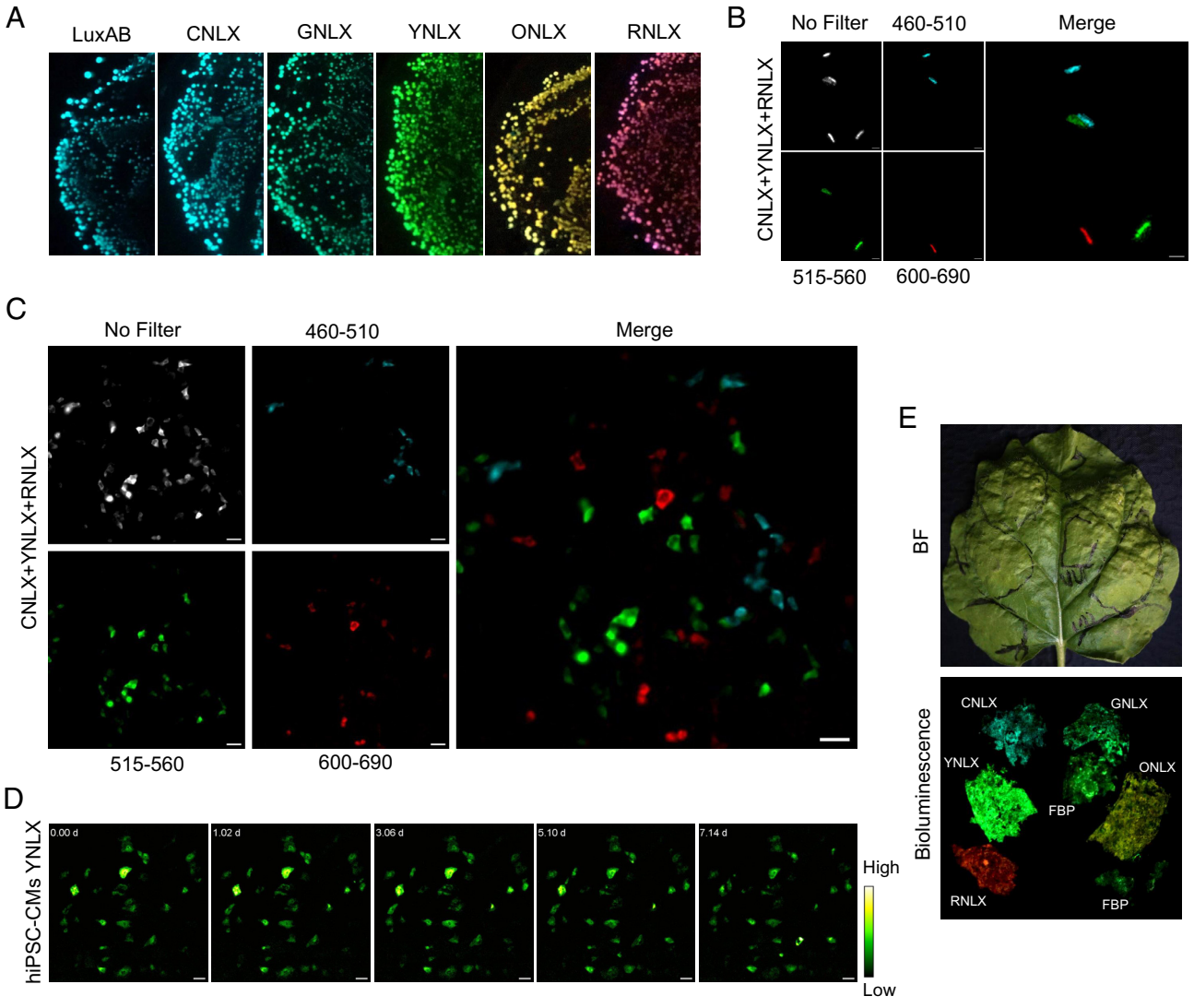

Fig. 2. Multicolor auto-bioluminescence imaging with NLXs. (*A*) Auto-bioluminescence images of *E. coli* expressing all NLX variants. Bioluminescence images were acquired using a Sony α7s camera with 10 s of exposure time. (*B*) Auto-bioluminescence imaging of mixed *E. coli* expressing CNLX, YNLX, or RNLX. Pseudocolor images, scale bars, 2 μm:100× magnification with 8 min of exposure time. (*C*) Auto-bioluminescence imaging of mixed HEK293T cells expressing CNLX, YNLX, or RNLX. Pseudocolor images, scale bars, 50 μm:40× magnification with 60 s of exposure time. (*D*) Long-term auto-bioluminescence imaging of hiPSC-CMs expressing YNLX. Pseudocolor images, scale bars, 100 μm:20× magnification with 4 min exposure time. (*E*) Auto-bioluminescence of *Nicotiana benthamiana* leaves expressing NLXs genes and fungal bioluminescence pathway (FBP). Bioluminescence images were acquired using a Sony α7s camera with 60 s of exposure time.

NLXs plasmids into HEK293T cells. The luminescence of the introduced NLXs was confirmed by microscopy using an EM-CCD camera for single-cell imaging. It was also shown that each luminescence color could be separated using specific optical filters (*SI Appendix*, Fig. S7*A*). Subsequently, we performed multiplex auto-bioluminescence imaging by mixing HEK293T cells expressing CNLX, YNLX, and RNLX (Fig. 2*C*). As with the mixed *E. coli* results, the cells could be distinguished by their respective wavelengths using spectral unmixing. We also conducted multiplex auto-bioluminescence imaging of subcellular structures by fusing RNLX with histones (H2B-RNLX) and YNLX with the plasma membrane (Lyn-YNLX), expressing them in HEK293T cells (*SI Appendix*, Fig. S7*B*). The luminescence signals from H2B-RNLX and Lyn-YNLX were separated by optical filtering and successfully showed correct localization.

In comparison, we attempted to check the luminescence dynamic of NIH3T3 cell transiently expressing YeNL and YNLX. YeNL was localized in both the cytosol and nucleus, while YNLX was only observed in the cytosol due to its larger size. The transfection efficiency of YNLX was lower than YeNL due to the need for three plasmids (YNLX, BF(G4S), and DEC(KZK)) to produce auto-bioluminescence (*SI Appendix*, Fig. S8 and Movie S1). YeNL showed higher luminescence after the addition of furimazine, but it decreased completely at 45 min and showed no luminescence at 18 h. In contrast, YNLX showed stable luminescence activity even at 18 h of observation (*SI Appendix*, Fig. S8).

We subsequently checked the ability of YNLX to promote long-term imaging in mammalian cells. We used human-induced pluripotent stem cell-derived cardiomyocytes (hiPSC-CMs) to transiently express YNLX. Mature cardiomyocytes are nondividing cells, preventing the loss of transfected DNA due to dilution of DNA by cell division (26). Thus, hiPSC-CMs are suitable for the expression of the NLX plasmid without genome integration (27). We successfully conducted continuous time-lapse auto-bioluminescence imaging of hiPSC-CMs expressing YNLX over one wk. demonstrating sustained auto-bioluminescence and beating activity (Fig. 2*D*, and Movies S2 and S3). This establishes YNLX as highly suitable for bioluminescence imaging in cardiac disease modeling, a critical area where hiPSC-CMs are indispensable.

We discovered that these optimized constructs could be transiently expressed in plant hosts without being optimized for plant codon usage. As a result of introducing the co lux operon constructs into the leaves of *N. benthamiana*, auto-bioluminescence from the leaves was successfully detected (Fig. 2*E* and *SI Appendix*, Fig. S9*A*). It also showed that NLXs produced luminescence intensities comparable to those of FBP (28) (*SI Appendix*, Fig. S9*B*). No significant differences were observed in the gene expression levels of NLXs and nnLuz (*SI Appendix*, Fig. S9*C*). Compared to nnLuz, which generates a single color, our NLXs, capable of producing multicolor auto-bioluminescence, serve as versatile reporter genes for plant research. Thus, the NLX-based Lux operon demonstrated multiplex auto-bioluminescence observations in various living organisms.

Application of NLXs as Gene Expression Reporters. Luciferase-based probes such as *Renilla* luciferase (Rluc) and firefly luciferase (Fluc) (29) have been widely used as reporter genes. However, luciferase-based probes still rely on luciferin addition. Thus, the ability to monitor the dynamics of reporter genes at the single-cell level for long-term observation without a decrease in luminescence intensity is limited. To evaluate whether our NLXs can also be used in reporter gene assays, we carried out a Wnt-reporter assay utilizing the Wnt-responsive promoter 7× TCF(5). The addition of LiCl as an agonist chemical to the Wnt protein resulted in luminescence

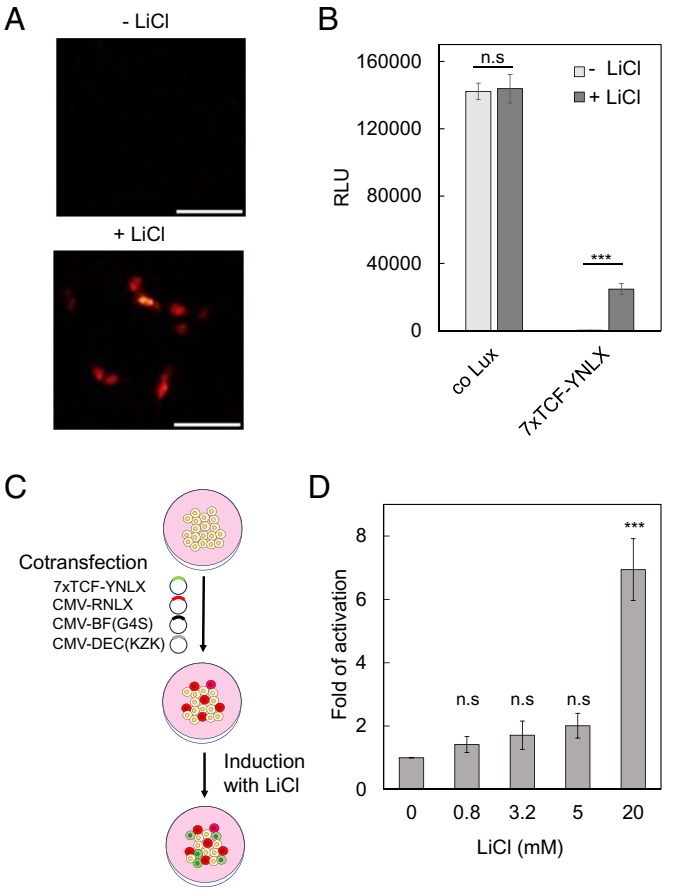

Fig. 3. Applications of NLXs in gene expression. Reporter assay for Wnt gene expression by YNLX. Auto-bioluminescence imaging (*A*) and auto-bioluminescence intensity (*B*) of HEK293T cells expressing co lux and 7× TCF-YNLX were measured at 16 h with or without the addition of 40 mM LiCl. Pseudocolor images, scale bars, 100 μm:20× magnification with 2 min exposure time. RLU is the relative light unit. Data are mean ± SD. n = 3, ***P <0.001. (*C*) Schematic of the multiplex assay. HEK293T cells transiently transfected with 7× TCF-YNLX, CMV-RNLX, and auto-bioluminescent parts (CMV-BF(G4S) and CMV-DEC(KZK)) plasmids were treated with LiCl to induce Wnt expression. (*D*) Auto-bioluminescence intensities of 7× TCF-YNLX upon the addition of various concentrations of LiCl. Bioluminescence intensities were measured 16 h after the addition of various concentrations of LiCl. Data are mean ± SD. n = 3, ***P <0.001

from the cell-encoded 7× TCF-YNLX plasmid (Fig. 3*A*). We also checked whether the addition of LiCl or Wnt-activation can affect the luminescence intensity of cells expressing Lux systems (co lux). No significant changes in auto-bioluminescence intensity were observed after the addition of LiCl compared to cells expressing the Wnt-responsive promoter 7× TCF (7× TCF-YNLX) (Fig. 3*B*). To track the dynamics of Wnt responsiveness at the single-cell level upon the addition of LiCl, we continued to express 7× TCF-YNLX in HEK293T cells for 16 h (*SI Appendix*, Fig. S10*A*). Bioluminescence was observed 4 h into the observation period and continued to be expressed (*SI Appendix*, Fig. S10*A* and Movie S4). Thus, the reporter gene based on YNLX was successfully used to monitor the dynamics of the reporter gene for long-term imaging.

We next demonstrated this reporter's utility in transient transfection for high-throughput screening (HTS) by cotransfecting CMV-RNLX and 7× TCF-YNLX in HEK293T cells, producing normalized data accounting for varying transfection efficiencies (Fig. 3 *C* and *D*). Unlike previous reporter assays utilizing Lux (30), which relied on Fluc or Rluc to normalize luminescence intensity and required cell lysis in downstream processes, our NLX system eliminates the need for additional luciferases and the requirement for cell lysis. This feature enhances convenience and

cost-effectiveness, making it particularly advantageous for HTS applications.

Application of NLXs as a Peptide-Based Indicator for Ions and Molecules. We expanded the application of Lux luciferase by developing a peptide-ligand-based indicator. To this end, we employed a ratiometric indicator strategy (Fig. 4*A*) to minimize signal drift due to changes in cell shape, focus drift, or variations in substrate consumption from auto-bioluminescence mechanisms. Consequently, we developed BRET-based indicators to detect crucial ligands such as calcium and ATP in living organisms. To develop a calcium indicator based on Lux, we fused the Ca^{2+}-sensitive troponin-C peptide (TnC) (31) into the site between Venus and LuxA in the YNLX plasmid. First, we screened Venus variants and circularly permutated Venus variants (32) to achieve the highest dynamic range upon Ca^{2+} addition (*SI Appendix*, Fig. S11). Among them, cp173Venus-TnC-LuxA (YNLX (Ca^{2+})) showed the largest dynamic range (181%) compared with the other variants (Fig. 4*B*). The K_d value for Ca^{2+} in this construct was 570 nM and the Hill coefficient was 1.02 (Fig. 4*C*). Furthermore, we observed Ca^{2+} changes after the addition of ionomycin and 10 mM $CaCl_2$ (Fig. 4*D*). Although the dynamic range of YNLX (Ca^{2+}) was lower than our prior Nano-lantern (Ca^{2+}) (5) and GeNL(Ca^{2+}) (6), which achieved dynamic ranges of approximately 300% and 500%, respectively, it still outperformed ratiometric indicators such as BRAC (33), which has a dynamic range of only 60%. YNLX (Ca^{2+})

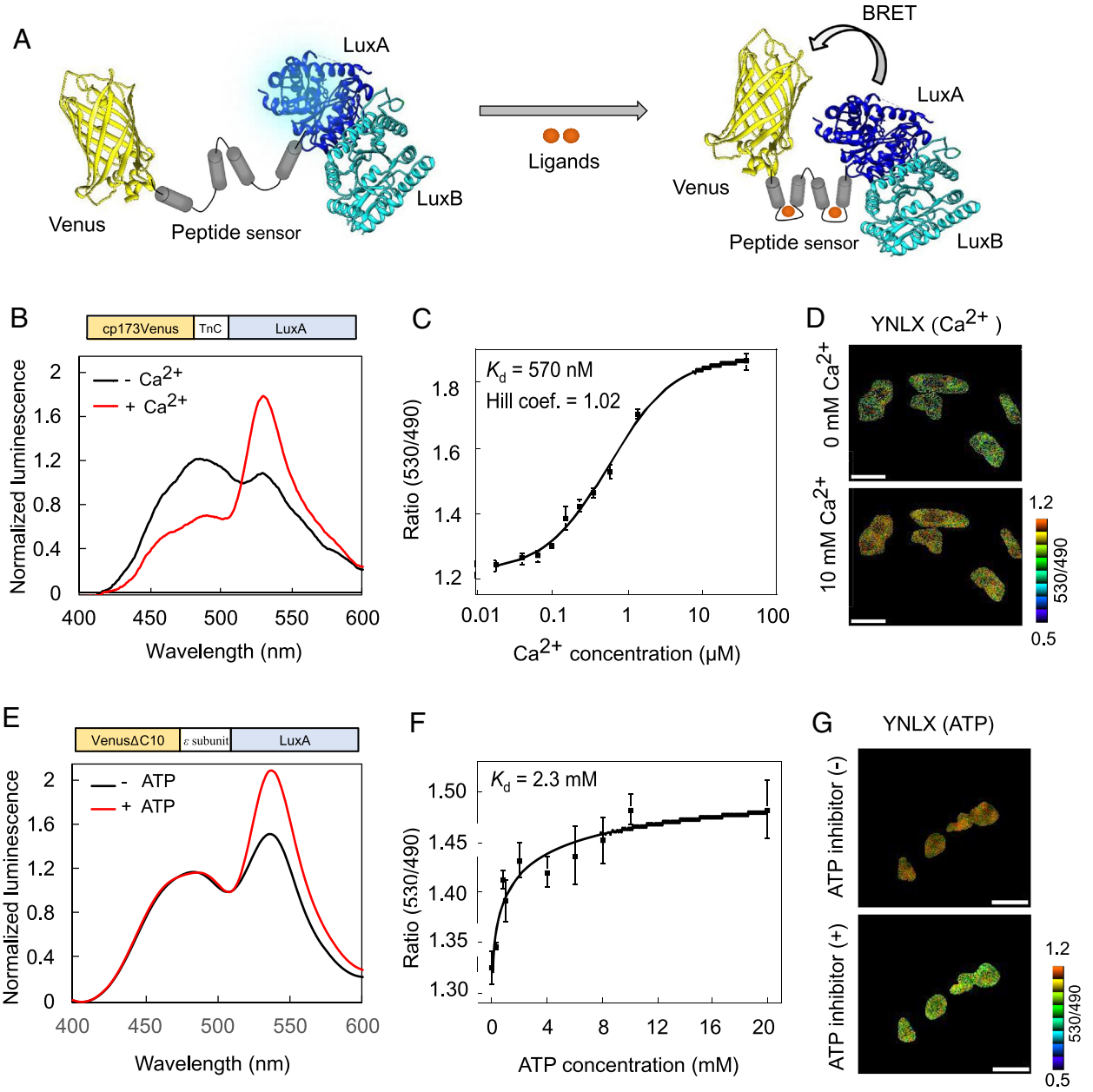

Fig. 4. Applications of NLXs as peptide-based sensors. (*A*) Schematics of peptide-based sensor based on NLXs with ratiometric strategy. (*B*) Emission spectra of YNLX (Ca^{2+}) with or without Ca^{2+}. Bioluminescence intensities were normalized by the isoemission point. (*C*) Ca^{2+} titration curve of YNLX (Ca^{2+}). The bioluminescence ratio was calculated from the peaks at 490 and 530 nm. (*D*) Auto-bioluminescence imaging of YNLX (Ca^{2+}). BRET ratio (pseudocolor images) of HEK293T cells expressing YNLX (Ca^{2+}) before and after addition of 10 μM ionomycin and 10 mM $CaCl_2$. Scale bars, 50 μm: 40× magnification with 2 min of exposure time. (*E*) Emission spectra of YNLX (ATP) with and without ATP. (*F*) ATP titration curve of YNLX(ATP). The bioluminescence ratio was calculated from the peaks at 490 and 530 nm. (*G*) Auto-bioluminescence imaging of YNLX (ATP). BRET ratio (pseudocolor images) of HEK293T cells expressing YNLX (Ca^{2+}) before and after the addition of an ATP inhibitor (20 μg/mL oligomycin A and 20 mM 2-deoxyglucose). Scale bars, 50 μm: 40× magnification with 3 min exposure time.

offered a dynamic range of 181% and a K_d value comparable to that of both Nano-lantern (Ca^{2+}) and GeNL (Ca^{2+}) at 620 and 480 nM, respectively (5, 6), demonstrating its functionality and comparability to existing non-autobioluminescent sensors (Fig. 4 *A*–*C*).

To develop an ATP indicator based on Lux, we fused the ε subunit (34) into the site between Venus and LuxA in YNLX, resulting in Venus-ε subunit-LuxA (YNLX (ATP)). YNLX (ATP) showed elevated BRET efficiency in the presence of ATP, with the K_d value for ATP of this construct being 2.3 mM (Fig. 4 *E* and *F*). YNLX (ATP) was designed as a low-affinity ATP sensor, making it is suitable for measuring physiological ATP level (1 to 5 mM) (35). Its K_d value was also comparable to that of previous non-auto-bioluminescent ATP indicators such as BTeam, which has a K_d value of 1.7 mM (36). We continued to evaluate the functionality of YNLX (ATP) in mammalian cell experiments. As a result, we successfully imaged intracellular ATP depletion upon addition of an inhibitor of ATP production (oligomycin and 2-deoxyglucose) (Fig. 4*G* and *SI Appendix*, Fig. S12). Therefore, YNLX was successfully applied as an ATP biosensor using a ratiometric strategy.

Discussion

Autonomous bioluminescence technology enables time-lapse imaging of biological processes without the need for luciferin. This technology eliminates the issue of luminescence decay and is cost-effective for HTS, making it an efficient option for luminescence imaging. However, the current state of auto-bioluminescent technology is primarily limited to observing individual biological phenomena, which hampers its utility for multiplexed autonomous imaging. Through the optimization of the LuxA position and BRET donor pairs, we successfully developed five color variants of auto-bioluminescence based on Lux luciferase. These color variants not only shifted the emission spectrum but also increased the luminescence intensity compared to that of the WT Lux. The cyan version, CNLX, is a brighter variant, potentially up to ten times brighter than the WT Lux, attributed to changes in QY influenced by the BRET phenomenon.

The successful imaging of auto-bioluminescence NLX in cellular systems is closely linked to the optimal pathways of auto-bioluminescent proteins within the cell. In bacterial expression systems, endogenous flavin reductase (Fre) (37) is constitutively expressed, making the addition of the *Frp* gene unnecessary in this host. However, in mammalian cells, Frp is essential for achieving high auto-bioluminescence (13). Nonetheless, $FMNH_2$, a substrate that is produced by Frp, undergoes rapid oxidation to FMN in the presence of dissolved oxygen in cell systems (38). To address this, we utilized a LuxB-Frp fusion (BF(G4S)) to facilitate the direct transfer of $FMNH_2$ to LuxA, thereby enhancing luminescence intensity in mammalian hosts (*SI Appendix*, Fig. S6).

The robustness of NLXs as multicolor auto-bioluminescent probes requires consideration of several factors, such as the expression level from transient expression. Despite optimizing three plasmids (NLX, BF(G4S), and DEC(KZK)) in mammalian cells to enhance transfection efficiency, these levels were not superior to those observed with single plasmid transfection, as we demonstrated in YeNL expression (*SI Appendix*, Fig. S8). Posttransfection observations did not indicate significant impacts on cell viability either immediately after 24 h in a CO_2 incubator or during a wk microscopic imaging, similar to previous studies (13, 39, 40). Other critical factors affecting autoluminescence intensity include optimal temperature (37 °C), cell condition, medium composition (free of nutrient deprivation, contamination, or toxic compounds), and the choice of promoter strength. To address emission spectral variations in NLXs, techniques like optical filtering, spectral unmixing and the use of CMOS-based cameras or phasor analysis (41) for bioluminescence imaging offer promising solutions for enhancing multiplexing capabilities.

The use of NLXs has enabled us to perform multiplex auto-bioluminescent imaging, overcoming the limitations of WT Lux and other auto-bioluminescent applications such as fungal luciferase (Luz). A notable feature of NLXs is their ability to facilitate auto-bioluminescence in various organisms, including bacterial, mammalian, and plant hosts. In comparison, the Luz system (FBP) is capable of fully establishing auto-bioluminescence in plant hosts. However, in the other hosts such as mammalian cells, this capability is limited due to inefficiencies in synthesizing caffeic acid as a luciferin precursor in their basal metabolic pathway (3). Additionally, our system contradicts the conventional belief that Lux causes low light intensity in the plant host (42). In fact, our findings revealed that we were able to grow transiently multicolor bright plants with light intensity comparable to FBP. This makes our system an ideal tool for plant research. Furthermore, we have expanded auto-bioluminescent applications, traditionally limited to single sensors, by developing subcellular tags, multiple gene assays, and a proof-of-concept peptide-based sensor for auto-bioluminescent Ca^{2+} and ATP imaging in longer observations. We are also focused on the importance of red-shifted emission of RNLX for imaging animal tissues. This is crucial because it allows for distinction from the signal absorption of deep tissues, particularly from hemoglobin (43, 44). In addition, the yellow-shifted emission of YNLX is essential for plant research because of its absorption spectrum of chlorophyll (45). Furthermore, the improvement in the enzymatic catalytic efficiency of LuxA through an increase in the k_{cat} value has the potential to significantly elevate its luminescence intensity, bringing it to a level comparable to that of eNL (6). Overall, we believe that our NLXs could be a "game-changing" development in bioluminescent technology, offering multipurpose applications in the future.

Materials and Methods

SI Appendix, SI Materials and Methods provided the details of the materials and methods used in this study, including of plasmid generation, luminescent characterization, cell culture, transient expression in plant leaves, and quantitative analysis of gene expression. In brief, NLXs and its modified genes were cloned into $pRSET_B$, pCDNA3.1(+), and pRI201-AN for bacterial, mammalian, and plant expression, respectively. Bioluminescence imaging was performed with an inverted microscope based on the IXplore™ Live for Luminescence (EVIDENT) system equipped with EM-CCD camera.

Nucleotide sequences of all constructs in this study are available in *SI Appendix*, Table S3.

Data, Materials, and Software Availability. All study data are included in the article and/or supporting information.

ACKNOWLEDGMENTS. We thank Prof. Stefan W. Hell for providing the co lux plasmids. We thank Dr. Kenji Osabe for the advice on luminescent protein characterization. This work was partly supported by grants from the Japan Science Technology Agency Core Research for Evolutional Science and Technology (JST CREST) (No. JPMJCR20H9 to T.N.), the Ministry of Education, Culture, Sports, Science and Technology (MEXT) (No. 18H05410 to T.N.), Japan Society for the Promotion of Science (No. 22H00409 to T.N.), New Energy and Industrial Technology Development Organization (No. 22681865 to T.N), and MEXT scholarship to S.H.K.

1. O. Shimomura, *Bioluminescence* (World Scientific, 2006).
2. H. Zhao *et al.*, Characterization of coelenterazine analogs for measurements of *Renilla* luciferase activity in live cells and living animals. *Mol. Imaging* **3**, 43–54 (2004).
3. A. A. Kotlobay *et al.*, Genetically encodable bioluminescent system from fungi. *Proc. Natl. Acad. Sci. U.S.A.* **115**, 12728–12732 (2018).
4. E. A. Meighen, Molecular biology of bacterial bioluminescence. *Microbiol. Rev.* **55**, 123–142 (1991).
5. A. Takai *et al.*, Expanded palette of nano-lanterns for real-time multicolor luminescence imaging. *Proc. Natl. Acad. Sci. U.S.A.* **112**, 4352–4356 (2015).
6. K. Suzuki *et al.*, Five colour variants of bright luminescent protein for real-time multicolour bioimaging. *Nat. Commun.* **7**, 13718 (2016).
7. L.Y.-C. Lin, R. Szittner, R. Friedman, E. A. Meighen, Changes in the kinetics and emission spectrum on mutation of the chromophore-binding platform in *Vibrio harveyi* luciferase. *Biochemistry* **43**, 3183–3194 (2004).
8. S. C. Daubner, A. M. Astorga, G. B. Leisman, T. O. Baldwin, Yellow light emission of *Vibrio fischeri* strain Y-1: Purification and characterization of the energy-accepting yellow fluorescent protein. *Proc. Natl. Acad. Sci. U.S.A.* **84**, 8912–8916 (1987).
9. V. N. Petushkov, B. G. Gibson, J. Lee, Direct measurement of excitation transfer in the protein complex of bacterial luciferase hydroxyflavin and the associated yellow fluorescence proteins from *Vibrio fischeri* Y1. *Biochemistry* **35**, 8413–8418 (1996).
10. E. Brodl, A. Winkler, P. Macheroux, Molecular mechanisms of bacterial bioluminescence. *Comput. Struct. Biotechnol. J.* **16**, 551–564 (2018).
11. Y. Sato *et al.*, Crystal structures of the lumazine protein from *Photobacterium kishitanii* in complexes with the authentic chromophore, 6,7-dimethyl- 8-(1′-D-ribityl) lumazine, and its analogues, riboflavin and flavin mononucleotide, at high resolution. *J. Bacteriol.* **192**, 127–133 (2010).
12. K. Saito *et al.*, Luminescent proteins for high-speed single-cell and whole-body imaging. *Nat. Commun.* **3**, 1262 (2012).
13. C. Gregor *et al.*, Autonomous bioluminescence imaging of single mammalian cells with the bacterial bioluminescence system. *Proc. Natl. Acad. Sci. U.S.A.* **116**, 26491–26496 (2019).
14. T. Nagai *et al.*, A variant of yellow fluorescent protein with fast and efficient maturation for cell-biological applications. *Nat. Biotechnol.* **20**, 87–90 (2002).
15. T. Kaku, K. Sugiura, T. Entani, K. Osabe, T. Nagai, Enhanced brightness of bacterial luciferase by bioluminescence resonance energy transfer. *Sci. Rep.* **11**, 14994 (2021).
16. J. Phonbuppha *et al.*, A Minimized chemoenzymatic cascade for bacterial luciferase in bioreporter applications. *Chem. BioChem* **21**, 2073–2079 (2020).
17. H. Tsutsui, S. Karasawa, Y. Okamura, A. Miyawaki, Improving membrane voltage measurements using FRET with new fluorescent proteins. *Nat. Methods* **5**, 683–685 (2008).
18. J. Goedhart *et al.*, Structure-guided evolution of cyan fluorescent proteins towards a quantum yield of 93%. *Nat. Commun.* **3**, 751 (2012).
19. J.-D. Pédelacq, S. Cabantous, T. Tran, T. C. Terwilliger, G. S. Waldo, Engineering and characterization of a superfolder green fluorescent protein. *Nat. Biotechnol.* **24**, 79–88 (2006).
20. D. S. Bindels *et al.*, mScarlet: A bright monomeric red fluorescent protein for cellular imaging. *Nat. Methods* **14**, 53–56 (2017).
21. J. Chu *et al.*, A bright cyan-excitable orange fluorescent protein facilitates dual-emission microscopy and enhances bioluminescence imaging in vivo. *Nat. Biotechnol.* **34**, 760–767 (2016).
22. S. Mukherjee, P. Manna, N. Douglas, P. P. Chapagain, R. Jimenez, Conformational dynamics of mcherry variants: A link between side-chain motions and fluorescence brightness. *J. Phys. Chem. B.* **127**, 52–61 (2023).
23. S. T. Gammon, W. M. Leevy, S. Gross, G. W. Gokel, D. Piwnica-Worms, Spectral unmixing of multicolored bioluminescence emitted from heterogeneous biological sources. *Anal. Chem.* **78**, 1520–1527 (2006).
24. N. Jawanda, K. Ahmed, S.-C. Tu, *Vibrio harveyi* flavin reductase—luciferase fusion protein mimics a single-component bifunctional monooxygenase. *Biochemistry* **47**, 368–377 (2008).
25. Y. Wang *et al.*, Optimization of a 2A self-cleaving peptide-based multigene expression system for efficient expression of upstream and downstream genes in silkworm. *Mol. Genet. Genomics* **294**, 849–859 (2019).
26. L. Cervera *et al.*, Generation of HIV-1 Gag VLPs by transient transfection of HEK 293 suspension cell cultures using an optimized animal-derived component free medium. *J. Biotechnol.* **166**, 152–165 (2013).
27. S. E. Bodbin, C. Denning, D. Mosqueira, Transfection of hpPSC-cardiomyocytes using ViaFect™ transfection reagent. *Methods Protoc.* **3**, 57 (2020).
28. A. Khakhar *et al.*, Building customizable auto-luminescent luciferase-based reporters in plants. *eLife* **9**, e52786 (2020).
29. A. Takai *et al.*, Anterior neural development requires Del1, a matrix-associated protein that attenuates canonical Wnt signaling via the Ror2 pathway. *Development* **137**, 3293–3302 (2010).
30. J. Phonbuppha, R. Tinikul, Y. Ohmiya, P. Chaiyen, High sensitivity and low-cost flavin luciferase (FLUXVc)-based reporter gene for mammalian cell expression. *J. Biol. Chem.* **299**, 104639 (2023).
31. T. Thestrup *et al.*, Optimized ratiometric calcium sensors for functional in vivo imaging of neurons and T lymphocytes. *Nat. Methods* **11**, 175–182 (2014).
32. T. Nagai, S. Yamada, T. Tominaga, M. Ichikawa, A. Miyawaki, Expanded dynamic range of fluorescent indicators for Ca^{2+} by circularly permuted yellow fluorescent proteins. *Proc. Natl. Acad. Sci. U.S.A.* **101**, 10554–10559 (2004).
33. K. Saito *et al.*, Auto-luminescent genetically-encoded ratiometric indicator for real-time Ca^{2+} imaging at the single cell level. *PLoS ONE* **5**, e9935 (2010).
34. H. Imamura *et al.*, Visualization of ATP levels inside single living cells with fluorescence resonance energy transfer-based genetically encoded indicators. *Proc. Natl. Acad. Sci. U.S.A.* **106**, 15651–15656 (2009).
35. H. Yaginuma *et al.*, Diversity in ATP concentrations in a single bacterial cell population revealed by quantitative single-cell imaging. *Sci. Rep.* **4**, 6522 (2014).
36. T. Yoshida, A. Kakizuka, H. Imamura, BTeam, a novel BRET-based biosensor for the accurate quantification of ATP concentration within living cells. *Sci. Rep.* **6**, 39618 (2016).
37. J. Akerboom *et al.*, Crystal structures of the GCaMP calcium sensor reveal the mechanism of fluorescence signal change and aid rational design. *J. Biol. Chem.* **284**, 6455–6464 (2009).
38. J. Lee, F. Müller, A. J. W. G. Visser, The sensitized bioluminescence mechanism of bacterial luciferase. *Photochem. Photobiol.* **95**, 679–704 (2019).
39. D. M. Close *et al.*, Autonomous bioluminescent expression of the bacterial luciferase gene cassette (lux) in a mammalian cell line. *PLoS ONE* **5**, e12441 (2010).
40. T. Xu, S. Ripp, G. S. Sayler, D. M. Close, Expression of a humanized viral 2A-Mediated lux operon efficiently generates autonomous bioluminescence in human cells. *PLoS ONE* **9**, e96347 (2014).
41. Z. Yao *et al.*, Multiplexed bioluminescence microscopy via phasor analysis. *Nat. Methods* **19**, 893–898 (2022).
42. A. Krichevsky, B. Meyers, A. Vainstein, P. Maliga, V. Citovsky, Autoluminescent plants. *PLoS ONE* **5**, e15461 (2010).
43. A. Dragulescu-Andrasi, C. T. Chan, A. De, T. F. Massoud, S. S. Gambhir, Bioluminescence resonance energy transfer (BRET) imaging of protein–protein interactions within deep tissues of living subjects. *Proc. Natl. Acad. Sci. U.S.A.* **108**, 12060–12065 (2011).
44. J. Chu *et al.*, Non-invasive intravital imaging of cellular differentiation with a bright red-excitable fluorescent protein. *Nat. Methods* **11**, 572–578 (2014).
45. Y. Furuhata, A. Sakai, T. Murakami, A. Nagasaki, Y. Kato, Bioluminescent imaging of *Arabidopsis thaliana* using an enhanced nano-lantern luminescence reporter system. *PLoS ONE* **15**, e0227477 (2020).